COLLINEAR CLUSTER TRI-PARTITION: CURRENT STATUS OF STUDIES

D.V. Kamanin[1], Yu.V. Pyatkov[1,2], A.A. Alexandrov[1], I.A. Alexandrova[1], N. Jacobs[3], N.A. Kondratyev[1], E.A. Kuznetsova[1], V. Malaza[3], O.V. Strekalovsky[1], V.E. Zhuchko[1]

[1]Joint Institute for Nuclear Research, Dubna, Russia
[2]Moscow Engineering Physics Institute, Moscow, Russia
[3]University of Stellenbosch, Faculty of Military Science, Military Academy, Saldanha 7395, South Africa

"Ni"–BUMP AND ITS INTERNAL STRUCTURE

In our recent publications [1] we have presented experimental evidences of existing of a new type of ternary decay of heavy low excited nuclei called by us collinear cluster tri-partition (CCT). The results were obtained in the frame of the "missing mass" approach. It means that only two from at least three decay partners were actually detected whereas a total mass of these fragments being less the mass of mother system serves a signature of multibody decay. Evidently direct detection of all CCT products proves to be a most convincing experimental approach but much complicated one because mosaic detection systems must be used to achieve the goal.

COMETA (Correlation Mosaic E–T Array) setup aimed at studying of rare multibody decays was put into operation recently in the Flerov Laboratory of the JINR. It is a double arm time-of-flight spectrometer which includes micro-channel plate (MCP) based "start" detector with the ^{252}Cf source inside, two mosaics of eight PIN diodes each and a "neutron belt" comprises 28 ^{3}He filled neutron counters. Below we discuss some results obtained at the COMETA setup.

LIGHT CHARGE PARTICLES ACCOMPANIED CCT: SPECTATORS OR PARTNERS OF THE DECAY?

We report here some results of three different experiments (marked Ex1, Ex2, Ex3 below) devoted to the search for collinear cluster tri-partition of ^{252}Cf (sf). The TOF–E (time-of-flight vs. energy) method for the measurements of two FF masses in coincidence with detectors placed at 180 degrees was used in all three experiments. In this method, the fragment velocities V, obtained by means of TOF and the energy E are measured for each detected fragment individually. Only two fragments were actually detected in each fission event (in two detectors, at 180^0) and their total mass, the sum M_s will serve as a sign of a multi-body decay, if it is significantly smaller than the mass of the initial system ("missing mass" method).

The most pronounced manifestation of the CCT as a missing mass event is a bump (fig. 1) in the two dimensional of the mass-mass correlation plot [1]. In this distribution of the fission fragment masses the bump occurs in one of the spectrometer arms with dispersive media (M_1), whereas it is absent in the analogues variable for the second arm (M_2). The bump is marked by the arrow in fig. 1a. We see two great bumps due to binary fission; the pronounced vertical and horizontal intensities are due to binary fission fragments scattered from the entrance support grid for the windows of the gas detectors. The FF mass correlation plot similar to that

obtained in Ex1 (fig. 1a) is shown in fig. 2a. Projections of this distribution both on the M_1 axis and on the M_s = const directions are presented in fig. 2b, and c, respectively. They are compared with the analogous spectra from the experiments Ex1 including the result from the ^{235}U(n_{th}, f) reaction [1]. The bump in the projected FF mass correlation data in fig. 2b is centered on mass (68÷70) amu, associated with magic isotopes of Ni. This bump will be called below as the "Ni"–bump. The bump marked by the arrow in fig. 2a looks less pronounced as compared to that obtained in Ex1 (fig. 1a). This can be partially explained by a worse mass resolution due to the wide-aperture avalanche counter used as "start" detectors in Ex2, instead of the MCP based detector in Ex1. Projections for Ex2 are shown in the "difference" version, i.e. as a difference of the tail regions in arm1 and in arm2, respectively. Overall a good agreement is observed in the position of the peaks in fig. 2b, and c for all three experiments. The shift of the peak for the ^{235}U(n_{th}, f) reaction in fig. 2c has already been discussed in ref. [1].

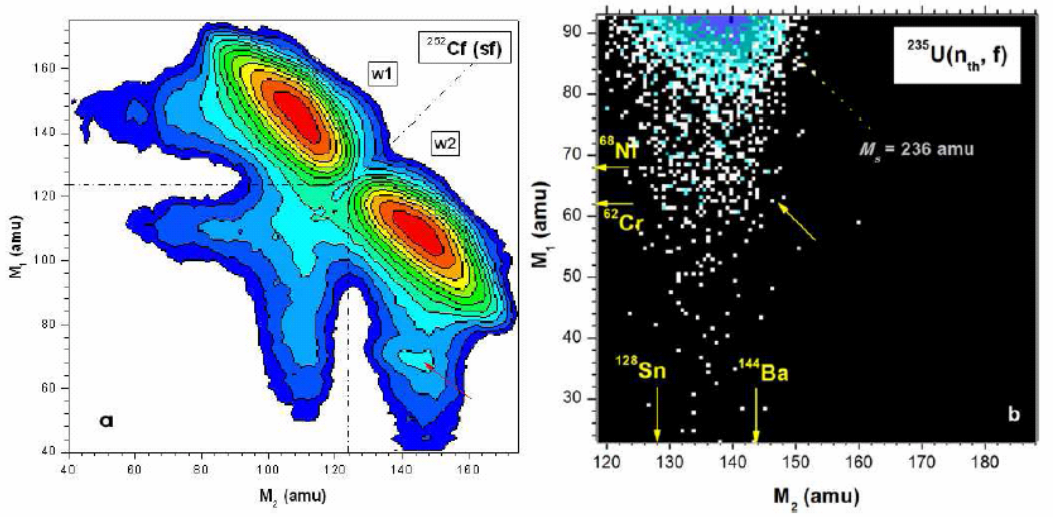

FIGURE 1. a) Contour map (in logarithmic scale, the steps between the lines are approximately a factor 2.5) of the mass-mass distribution of the collinear fragments of ^{252}Cf (sf), detected in coincidence in the two opposite arms of the FOBOS spectrometer. The specific bump in arm1 is indicated by an arrow. Two large windows *w*1 and *w*2 are used in the later analysis (section 4). b) The region of the mass distribution for the FFs from the reaction ^{235}U(n_{th}, f) around the bump. The bump is bounded by magic clusters (marked by corresponding symbols near the axes). The tilted arrow shows a valley between the ridges $M_1 + M_2$ = 210 amu of M_s = const. See text for details.

The methodically quite different experiment Ex3 shows results, which confirm our previous results concerning the structures in the missing mass distributions. In this case there is no tail due to scattering from material in front of the *E*-detectors. Fig. 3 shows the region of the mass distribution for the FFs from ^{252}Cf (sf) around the "Ni"–bump (M_1 = 68÷80 amu, M_2 = 128÷150 amu). The structures are seen in the spectrometer arm facing the source backing only. No additional selection of the fission events has been applied in this case; the experiment has no background from scattered FFs. A rectangular-like structure below the locus of binary fission is bounded by magic nuclei (their masses are marked by the numbered arrows) namely ^{128}Sn (1), ^{68}Ni (2), ^{72}Ni (3). Two tilted diagonal lines with M_s = 196 amu and M_s = 202 amu (marked by number 4) start from the partitions 68/128 and 68/134, respectively. In experiment Ex1 [1], Figure 6, similar sub-structures have been seen for masses M_s = 204, 208, 212, 214 amu where they were revealed indirectly by the applying of

the second derivative filter, but in the absolutely statistically reliable distribution ("Ni"–bump) processed. Bearing in mind essential difference in the geometry of blocking mediums in Ex1 and Ex3 to be decisive for the relative experimental yields of the CCT modes with different angular distributions between the fragments forming the fork flying in the same direction the preference of lighter partitions standing behind the tilted ridges in Ex3 is not strange. Positions of the points in the lower part of fig. 3 do not contradict to possible existence of all the ridges revealed in Ex1 if the following magic partitions are assigned to their beginnings: 70/134, 68/140, 68/144, 70/144.

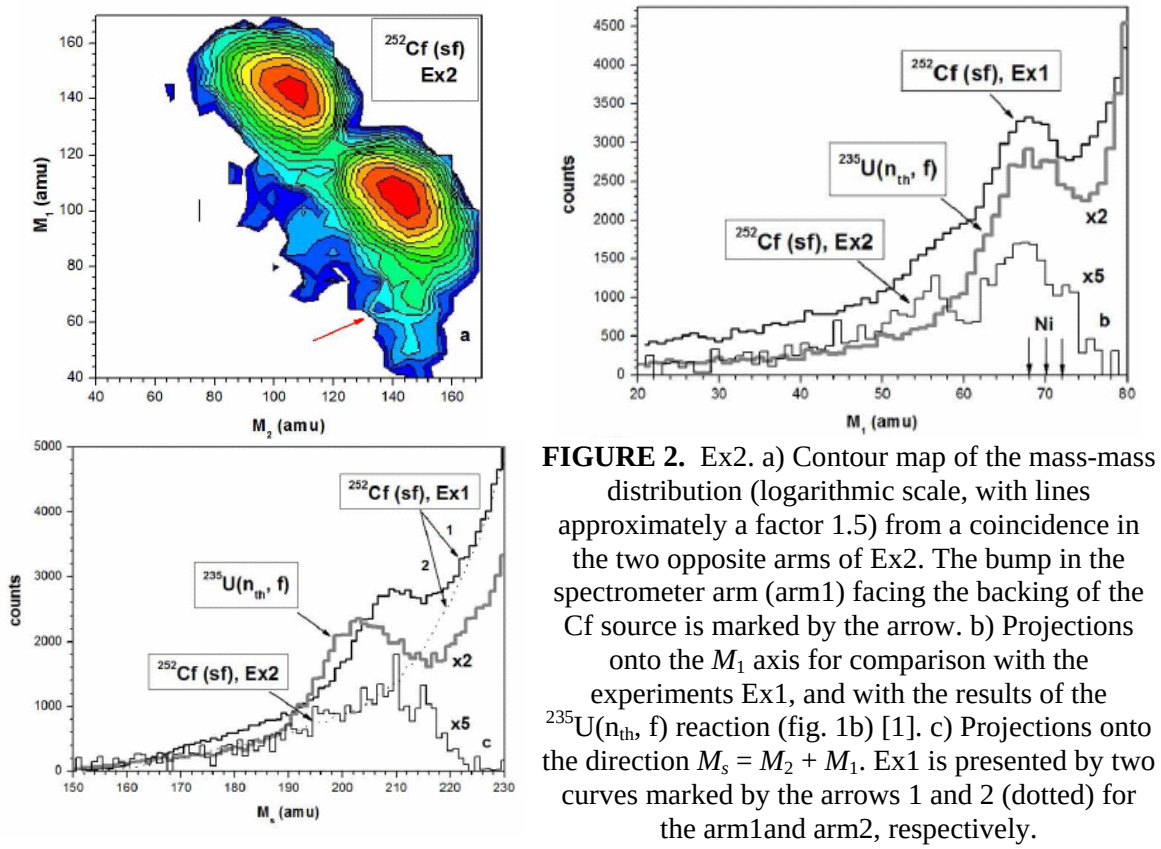

FIGURE 2. Ex2. a) Contour map of the mass-mass distribution (logarithmic scale, with lines approximately a factor 1.5) from a coincidence in the two opposite arms of Ex2. The bump in the spectrometer arm (arm1) facing the backing of the Cf source is marked by the arrow. b) Projections onto the M_1 axis for comparison with the experiments Ex1, and with the results of the ^{235}U(n$_{th}$, f) reaction (fig. 1b) [1]. c) Projections onto the direction $M_s = M_2 + M_1$. Ex1 is presented by two curves marked by the arrows 1 and 2 (dotted) for the arm1and arm2, respectively.

Thus, comparison of Ex1 and Ex3 which are absolutely different both by the detectors and mass calculation procedures used as well as the statistics collected delivers strong confirmation of the existence of tilted ridges M_s = const linked with magic partitions. As can be inferred from fig. 3, the yield of the FFs with the mass 128 amu, which is extremely low in conventional binary fission, is clearly seen. It means that scattered binary fragments in any case cannot give rise to this structure. A part of the plot just below the locus of the binary FFs is shown in a larger scale in the insert. The structure is bounded by the magic nuclei of ^{80}Ge, ^{78}Ni, ^{132}Sn, ^{144}Ba (their masses are marked by the arrows 5, 6, 7, 8, respectively). The observations presented point to the fact that the CCT decay occurs in a variety of modes (mass combinations), which could not be distinguished in Ex1 without additional gating due to the large background from scattered FFs. Likely due to the difference in the parameters of the blocking mediums the yield of the "Ni"–bump in Ex3 does not exceed 10^{-3} per binary fission i.e. much less then inEx1 and Ex2. At the same time with the absence of scattered FFs in Ex3, allowed the observation of the internal structure, without any additional cleaning of the FF mass distribution.

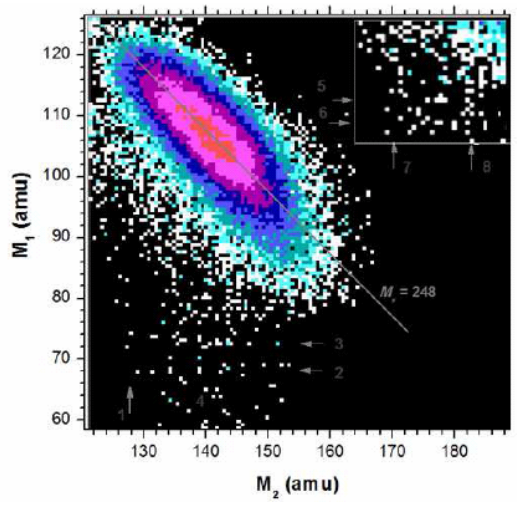

FIGURE 3. Results of Ex3: The region of the mass-mass distribution for the FFs from ^{252}Cf (sf) around the CCT bump (figs. 1a and 2a). No additional gates were applied. An internal structure of the bump as the straight lines (marked by the arrows) is seen in fig. 2c, as a projection. A part of the plot just below the locus of binary FFs produces the rectangular structure seen before. It is shown in the insert in a larger scale.

SOMETHING NEW IN "BUMPOLOGY"

Above we have discussed the "Ni"–bump, which is vividly seen in the FFs mass-mass correlation plot without any processing (fig. 1), because it is located below the loci of binary fission. As was stressed in ref. [1] the bump shows internal structure consisting of two different sequences of ridges namely $M_s = M_1 + M_2 = \text{const}$ (tilted ridges) and $M_1 = \text{const}$ (where M_1 is the lighter fragment among two detected). In the neutron gating data obtained at the modified FOBOS and COMETA spectrometers [2] we have observed rectangular structures bounded by magic clusters not only spherical (Ni, Ge) but also deformed ones (^{98}Sr, ^{108}Mo). This observation gave hints that in the data of Ex1 deformed light clusters could manifest themselves as well. In order to peruse this idea we have reanalyzed the data of Ex1, namely the M_1–M_2 distribution (fig. 1a), in this figure we choose two large windows *w*1 and *w*2. The corresponding projections of the distributions onto the coordinate axis in the "clean" arm2 (box *w*1) and those facing to the source backing, arm1 (box *w*2), are compared in Figure 4a. The spectra were normalized to the same number of counts. The difference spectrum is shown in fig. 4b). Some statistically significant peaks are seen. The first one from the left is the projection of the "Ni"–bump onto the M_1 axis. Further structures follow: a wide peak bounded by magic nuclei of ^{82}Ge and ^{94}Kr (deformed), and peaks centering, respectively, at ^{98}Sr and ^{108}Mo isotopes (both to be magic and deformed).The origin of the peaks becomes clear from following consideration illustrated by fig. 5. Let us focus our attention on the peak in the vicinity of mass 70 amu (Ni) in the difference spectrum (right part of the "Ni"–bump, fig. 4b). The fact that the "Ni"–bump is observed only in one of the spectrometer arms facing the source backing was treated above as being due to a stopping in the entrance mesh of the ionization chamber of the third light fragment directed in the same arm as the Ni cluster. In contrast, the same pair of fragments directed at the "clean" arm2 predominantly (due to a low angular divergence) gives overlapping energy signals in the "stop" detector and time-of-flight signals corresponding to the faster of them. As a result the calculated mass will be incorrect but registered as an "almost normal" binary decay within the experimental mass dispersion. Such events from arm2 play a role of "donors" for the bump events in arm1. In other words the events being actually ternary should move from the locus defined as binary in arm2 to the "Ni"–bump in arm1 (illustration in the upper part of fig. 4d). As a result the difference

spectrum $Y(w2)–Y(w1)$ (low part of fig. 4d) must have the peak of positive counts and corresponding negative counting tail for the “donors” fragments in the region of binary fission. Evidently the yields of the bump and the “tail” must be equal to each other. In the experiment one observes a superposition of partial contributions from different magic clusters. For instance, the gross central peak in fig. 4b lies on the negative “background” (tail) provided by all less massive magic clusters. The position of the local peaks in fig. 4b could depend from a possible shift in the centers of the spectra in fig. 4a due to independent mass calibrations in the opposite arms of the spectrometer. We have two independent evidences for the required quality of the calibrations. The maximal mass of the light fragment in the mass-asymmetric fission mode cannot exceed 120 amu due to the known extreme stability of the complimentary heavy fragment (double magic ^{132}Sn nucleus). This is just the feature observed in fig. 4b: the negative yield in the difference spectrum vanishes for the mass partition 120/132 amu. The negative minimum at $M_c/2$ (fig. 4b where M_c is the mass of the fissioning nucleus of ^{252}Cf, shows, that ternary fragmentation is likely to occur in the region of mass-symmetric fission as well. Another argument for the quality of the mass calibrations can be inferred from fig. 4c. The figure shows the second derivative of the mass spectrum linked with the box $w2$ of the data from Ex1 this shows similar peaks as the difference spectrum in fig. 4b. Thus fig. 4b can be treated as a manifestation of a whole sequence of bumps, based on magic spherical and deformed clusters of ^{68,70}Ni, ^{82}Ge, ^{94}Kr, ^{98}Sr, ^{102}Zr, ^{108}Mo, ^{111}Tc. The yield of the most populated “Mo”–bump (A = 106 (111) is about 8×10^{-3}per binary fission, i.e. twice as high as the corresponding value for the “Ni”–bump directly seen in the mass correlation plot (fig. 1a).

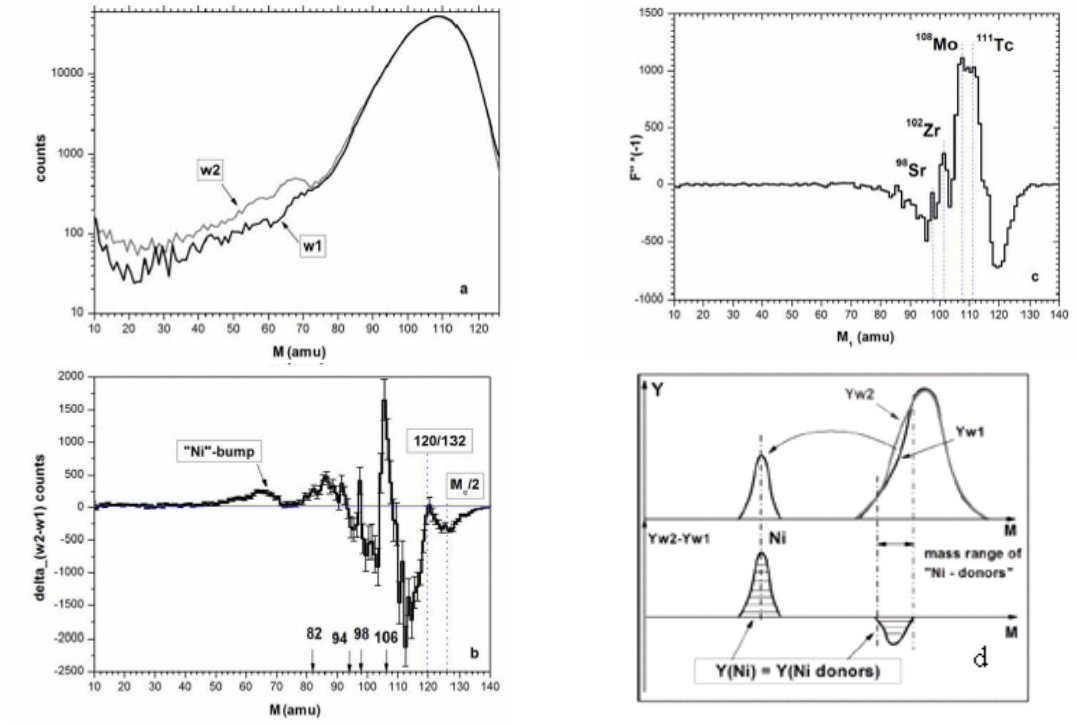

FIGURE 4. a) Projections of the events from box $w1$ and box $w2$ (Ex1, shown in fig. 1a onto M_2 and M_1 axes, respectively; b) difference between these projections and, c) the second derivative of the spectrum being the projection of the events from box $w2$ onto M_1 axis, d) schematic representation of fig. 4) (upper part of the figure) for illustrating a reason of forming a negative tail of the “Ni”–bump in the difference spectrum of yields $Y(w2)–Y(w1)$ (lower part).

RESULTS ON TRUE TERNARY COINCIDENCES

In this section ternary events observed at the COMETA setup will be analyzed. It means that three fragments were really detected in coincidence in each event. The FFs from such events are labeled as m_1, m_2, m_3 in an order of decreasing masses in each ternary event. Mass correlation plot for the masses m_1, m_2 is shown in fig. 5. It is observed only for the events where the fork of two fragments was detected in the spectrometer arm faced to the source backing.

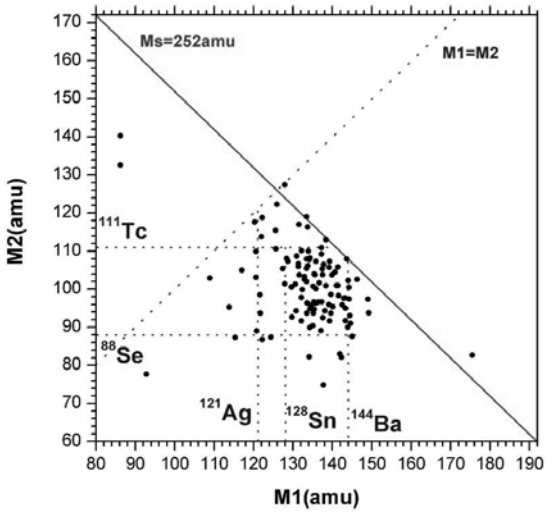

FIGURE 5. Correlation mass plot for two heavy partners of ternary decay. Rectangular structure in its center is bounded by the magic nuclei.

Rectangular structure bounded by the magic nuclei is seen in the center of the plot. Missing masses are ranged from 4 (alpha particle) up to 48 amu. Another distribution (fig. 6) is convenient for testing mass conservation law in ternary decays. Normally experimental points must lie on the line M_s = 252 amu (where M_s is a total mass of all three decay partners i.e. $M_s = m_1 + m_2 + m_3$) within mass resolution of the spectrometer. It is not so for the bulk of the points presented in the typical M_{s12}–m_3 distribution in fig. 6. It seems they form some families of events which met the condition $m_1 + m_2$ = const what corresponds to the fixed mass of the third fragment. But only part of this fragment was actually detected almost in all the events presented. For instance, presumable configuration for the events marked by the circle is shown in the insert of Figure 6. Likely the middle fragment of the initially three body chain was clusterized into two lighter fragments in the scission point and only one of them (^{14}C) was detected.

The following alternative scenario could give rise to the peculiarity mentioned (fig. 7). After first rupture, for instance, in the configuration shown in the insert of fig. 6, ^{132}Sn nucleus and di-nuclear system Ge/S become free. Then a break-up of the molecule appears to occur due to inelastic scattering in the backing of the source. As a result the scattered Ge nucleus and knocked out ion of ^{27}Al or ^{16}O can be detected in the corresponding spectrometer arm while the ^{40}S nucleus flies in the opposite direction following ^{132}Sn nucleus. Similar process with even larger energy is known as Coulomb fission [3]. The yield of such process is strongly dependent from the binding energy of the molecule and scattering angle. If the scenario under discussion is really realized a knocked out ion can be regarded as a specific spectator of the CCT process.

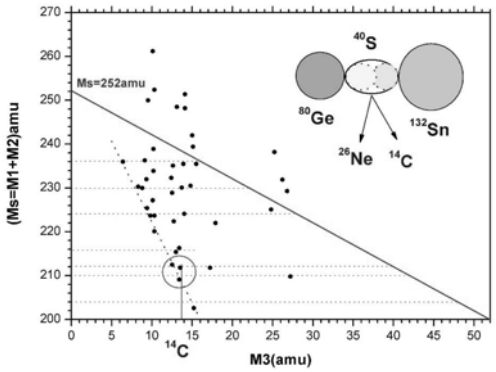

FIGURE 6. Typical distribution $M_{s12} = m_1 + m_2$ vs. m_3. Presumable pre-scission configuration for the events underlined by the circle is presented in the insert. See text for details.

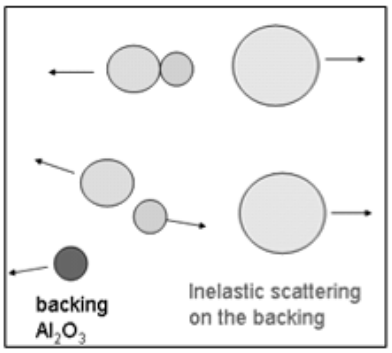

FIGURE 7. Possible way of forming a fork of two fragments flying in the same direction due to a breakup of the di-nuclear molecule in an inelastic scattering in the source backing.

Summing up, the results obtained at the COMETA setup on direct detecting of three partners of at least ternary decay of ^{252}Cf (sf) can be treated in the frame of two following hypothesis. The first one is that the light detected fragment (m_3) can be some part of the middle clusterized fragment of the three-body chain-like pre-scission configuration in the CCT channel. The second hypothesis treats m_3 as a mass of the ion knocked out from the source backing. The same inelastic scattering gives rise to the break-up of the di-nuclear molecule formed after first rupture of the pre-scission CCT configuration.

TO A UNIFIED MODEL OF TERNARY DECAYS OF LOW EXCITED NUCLEI

For the moment three different types of ternary decays of low excited nuclei are known, namely, conventional ternary fission, polar emission and CCT. It seems there is a deep link between the polar emission and CCT, at least with the CCT accompanied by a light charged particle [4]. It would be extremely interesting to compare all three ternary decays in the frame of the unified experimental approach. We are planning to do this by means of step by step increasing of the aperture of the COMETA spectrometer and the first step has been already done. Recently COMETA-2 set up (fig. 8) was put into operation at the FLNR of the JINR.

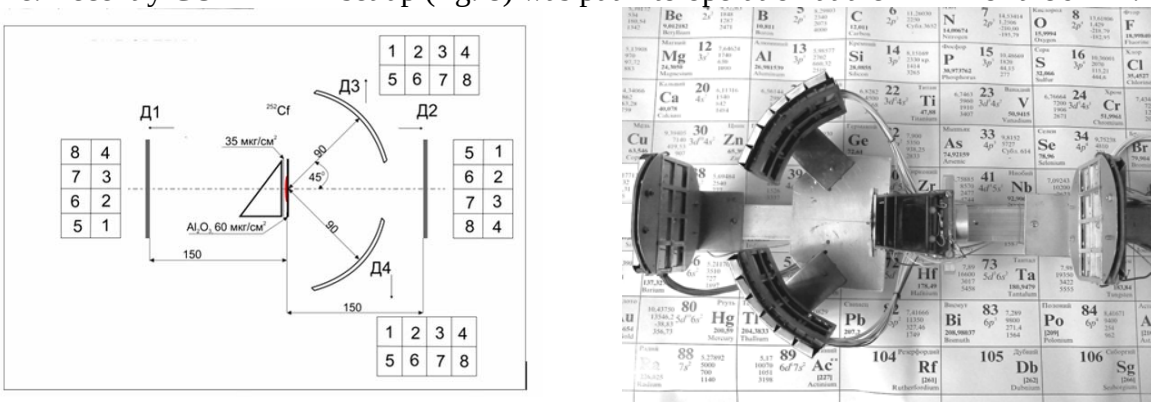

FIGURE 8. COMETA-2 setup. The scheme of the FFs detectors (left side) and their photo (right side).

It complains four mosaics of Si semiconductor detectors of eight diodes each and the micro channel plates based “start” detector with the ^{252}Cfi inside. The FFs detectors are surrounded by the “neutron belt” which was used previously at the COMETA spectrometer. Processing of the data of the test run is in progress.

CONCLUSIONS

1. New evidences were obtained in favor of conclusion that the CCT is due to the preformation of at least two magic clusters, deformed as well. The CCT modes based on these combinations are more preferable.
2. New experimental information obtained gives evidence of a nontrivial scenario of the collinear cluster tri-partition process and structure of the lightest decay partner especially.
3. Additional efforts are needed for studying of all known ternary decays in the frame of the unified experimental approach.

REFERENCES

1. Yu.V. Pyatkov et al. Eur. Phys. J. A 45 (2010) 29.
2. Yu.V. Pyatkov et al., submitted in Eur. Phys. J. A, (2011).
3. L. Wilets et al., Phys. Rev. 156 (1967) 1349
4. Yu.V. Pyatkov et al., Bulletin of the Russian Academy of Sciences. Physics, v. 75, (2011) 949.